Electronic Supplementary Material (ESI) for ChemComm.

Supporting Information

Electric Field-Driven Dual-Rotation in Molecular Motors: Insights from Molecular Dynamics Simulations

Bo Hu and Jin Wen*

State Key Laboratory for Modification of Chemical Fibers and Polymer Materials, College of Materials Science and Engineering, Donghua University, Shanghai 201620, China

E-mail: jinwen@dhu.edu.cn

Computational Methods

Electronic Structure Calculations

We aimed to investigate the impact of electric fields on the dynamic behavior of molecular motors, as determined by their static PESs. The PESs of different molecular motors are influenced by various factors, including charge distribution, substituent effects, and environmental conditions. To explore these influences on the PESs of molecular motors in their ground state, we employed density functional theory (DFT). Initially, we obtained the equilibrium configuration through geometry optimization at the BHandHLYP/cc-pVDZ level, which was validated by subsequent frequency calculations. Previous studies have indicated that the BHandHLYP functional yielded reasonable energy profiles for molecular motors along the isomerization reaction pathway.[1] Building upon this equilibrium structure, we conducted a relaxed scan along the dihedral angle of β (Figure S1a), ranging from 0° to 180° with 10° increments, to investigate the rotational profile of the molecular motor (Figure S2). We compared the PESs of the natural and charged molecular motors, including those with negative and positive charges. Additionally, single-point calculations were performed with and without the presence of an electric field along the rotational profiles to assess the rotational barrier. We applied an electric field of 5 V/nm along the z-axis direction (Figure S1b). All calculations were performed using the ORCA software package (Version 5.0.1).[2]

Classical MD Simulations

To investigate the influence of an external electric field on the motions of four molecular motors (illustrated in Scheme 1c), we employed all-atom molecular dynamics (MD) simulations. This study examined the influence of substituent groups, charge configuration, temperature, and electric field strength on the dynamic behavior of the molecular motors. Each molecular motor was solvated in a cubic box containing 1000 water molecules, initially measuring $5.34 \times 5.34 \times 5.34\,\mathrm{nm}^3$, to prevent steric hindrance between solvents and the molecular

motors. In the MD simulations, the general AMBER force field (GAFF)[3] and charges obtained from a restrained electrostatic potential (RESP)[4]fit at the BHandHLYP[5]/cc-pVDZ level were used for both the molecular motors and water molecules. The cubic solvation boxes were constructed using the TIP3P water model. A cutoff of 12 Å was implemented for short-range nonbonded interactions, and the particle mesh Ewald (PME)[6] was utilized to compute long-range electrostatic interactions. The LINCS algorithm was employed to restrain all covalent bonds involving hydrogen atoms.[7] Periodic boundary conditions were applied in all directions. We have conducted a comparative analysis of single-point energies along torsion β to calibrate the parameters employed in GAFF by comparing the rotational barriers predicted by GAFF with those obtained from BHandHLYP/cc-pVDZ level calculations, as depicted in Figures S3-S4. The rotational barriers calculated using GAFF are in close agreement with those from DFT calculations, with a maximum discrepancy of approximately 8 kcal/mol. This result confirms the validity of the GAFF parameters for the following dynamic simulations.

During MD simulations, energy minimization was first performed to ensure that the maximum force on each atom was below 500 kJ/(mol·nm). Subsequently, an annealing process was carried out in the NVT ensemble for 10 ns, employing the V-rescale[8] coupling method to ensure the simulation temperature reached the desired equilibrium state. Following the annealing simulation, the system was equilibrated within the NPT ensembles for 20 ns, with pressure maintained isotropically at 1.0 bar using the Berendsen coupling method.[9] Ultimately, we randomly selected 20 equilibrated configurations and produced MD simulations under an external electric field in the NVT ensemble for 5 ns, where the electric field direction was along the z-axis. All molecular dynamics simulations were performed by GROMACS v.2021.3.[10] Trajectory visualization and analysis were performed using the Visual Molecular Dynamics (VMD) package.[11]

Table 1: The dipole moment (Debye) under equilibrium states in different systems

	M1	M2	M3	M4
sc	2.41725	1.49926	1.33238	0.17907
ut	4.73926	1.65669	1.78214	0.72447

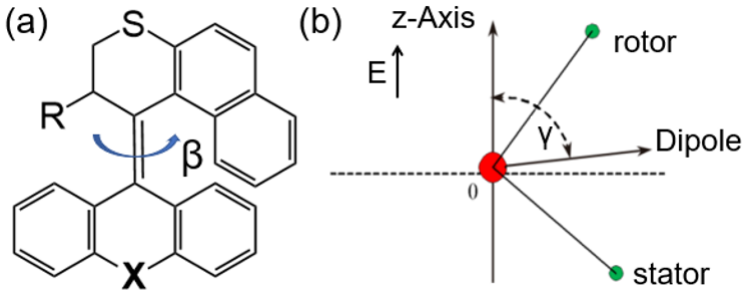

Figure S1: The definition of angles (a) central dihedral angle β (b) γ angle between the electric field and the molecular dipole.

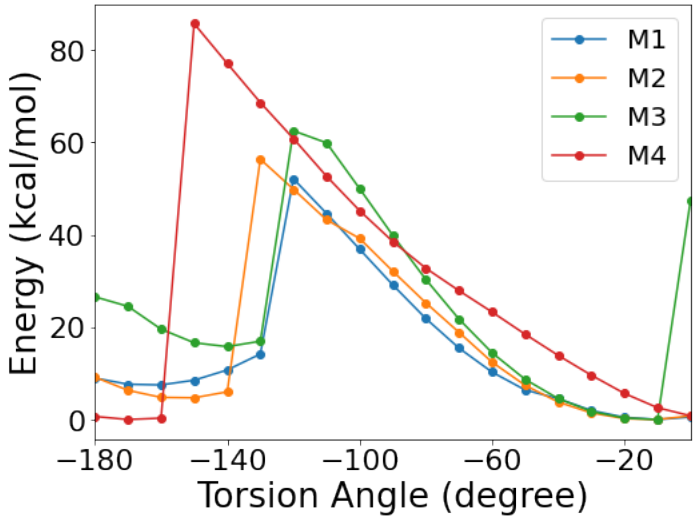

Figure S2: Ground state potential energy surfaces of M1, M2, M3, and M4 under ionization.

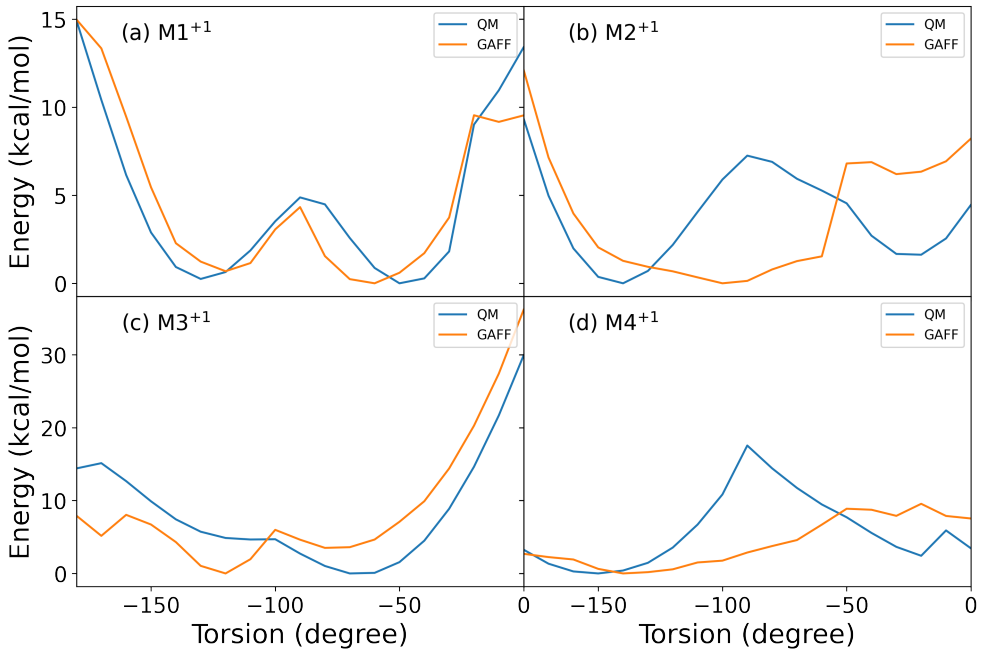

Figure S3: The rotational barriers predicted by GAFF and those obtained from BHandHLYP/cc-pVDZ level calculations are refined and compared across different systems (a) $\mathbf{M1}^{+1}$, (b) $\mathbf{M2}^{+1}$, (c) $\mathbf{M3}^{+1}$, (d) $\mathbf{M4}^{+1}$.

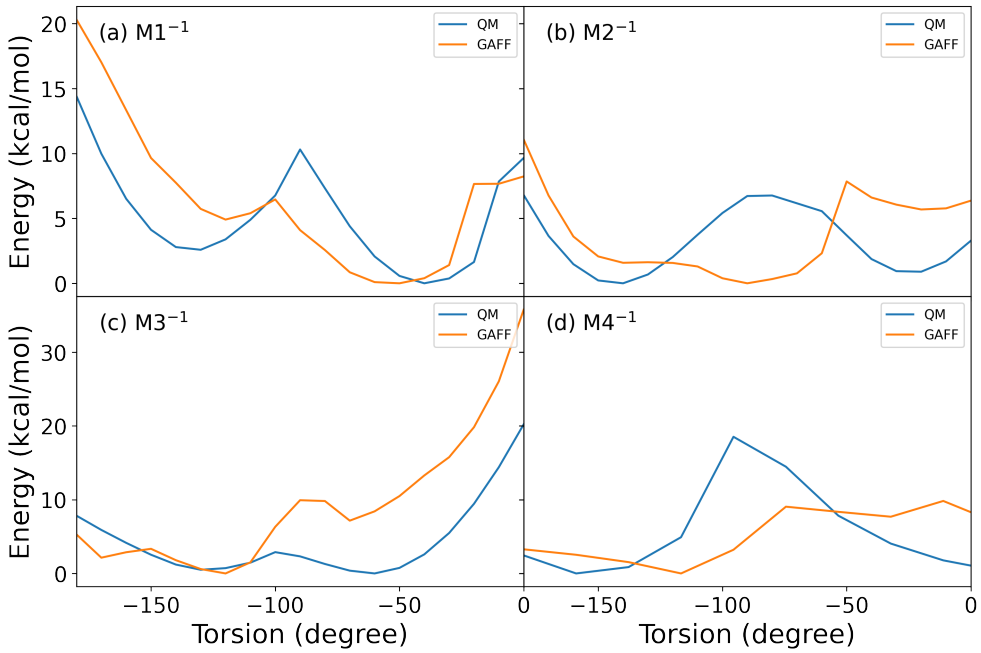

Figure S4: The rotational barriers predicted by GAFF and those obtained from BHandHLYP/cc-pVDZ level calculations are refined and compared across different systems (a) $\mathbf{M1}^{-1}$, (b) $\mathbf{M2}^{-1}$, (c) $\mathbf{M3}^{-1}$, (d) $\mathbf{M4}^{-1}$.

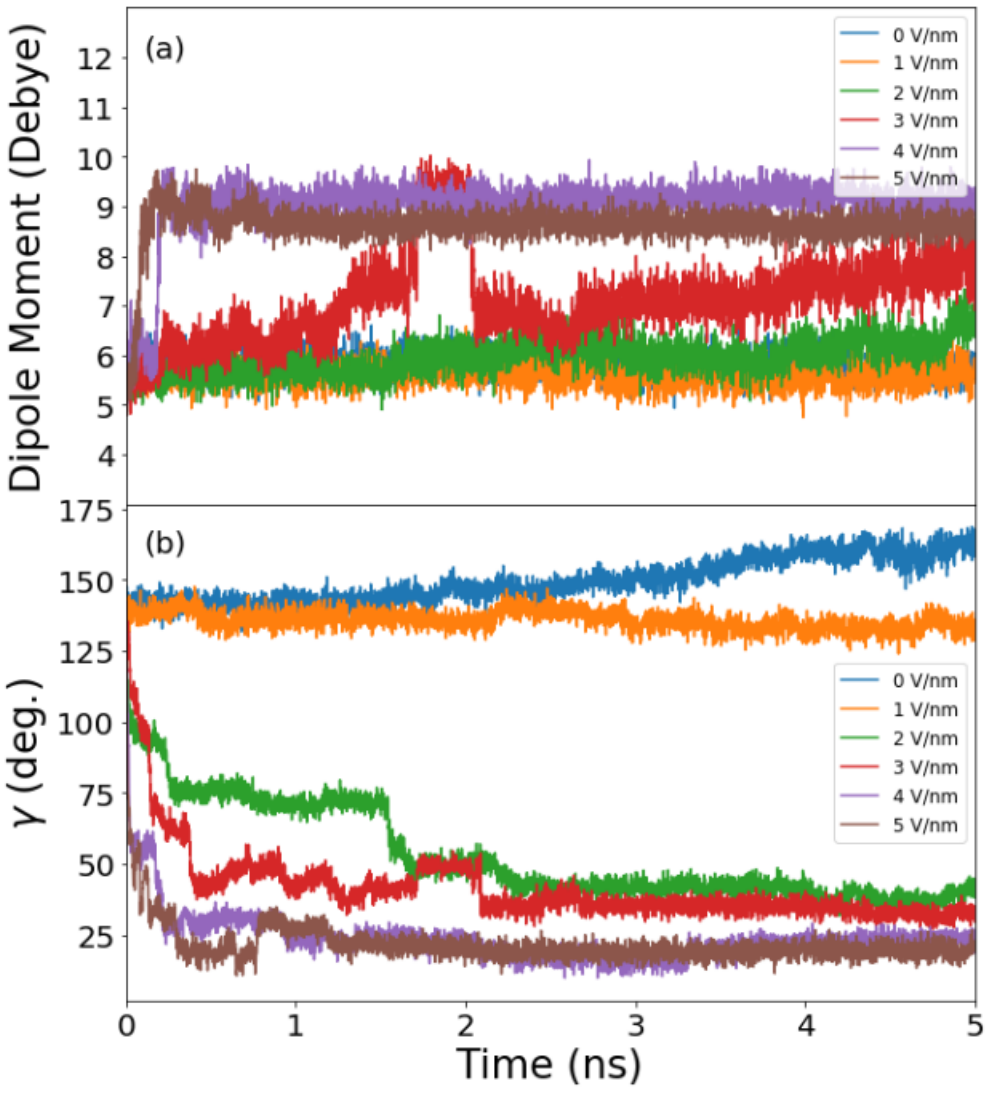

Figure S5: Time evolution of (a) the magnitude of the dipole moment under different electric fields, (b) angle between the dipole moment direction and the electric field direction for M1.

The simulation results of M1 under different conditions

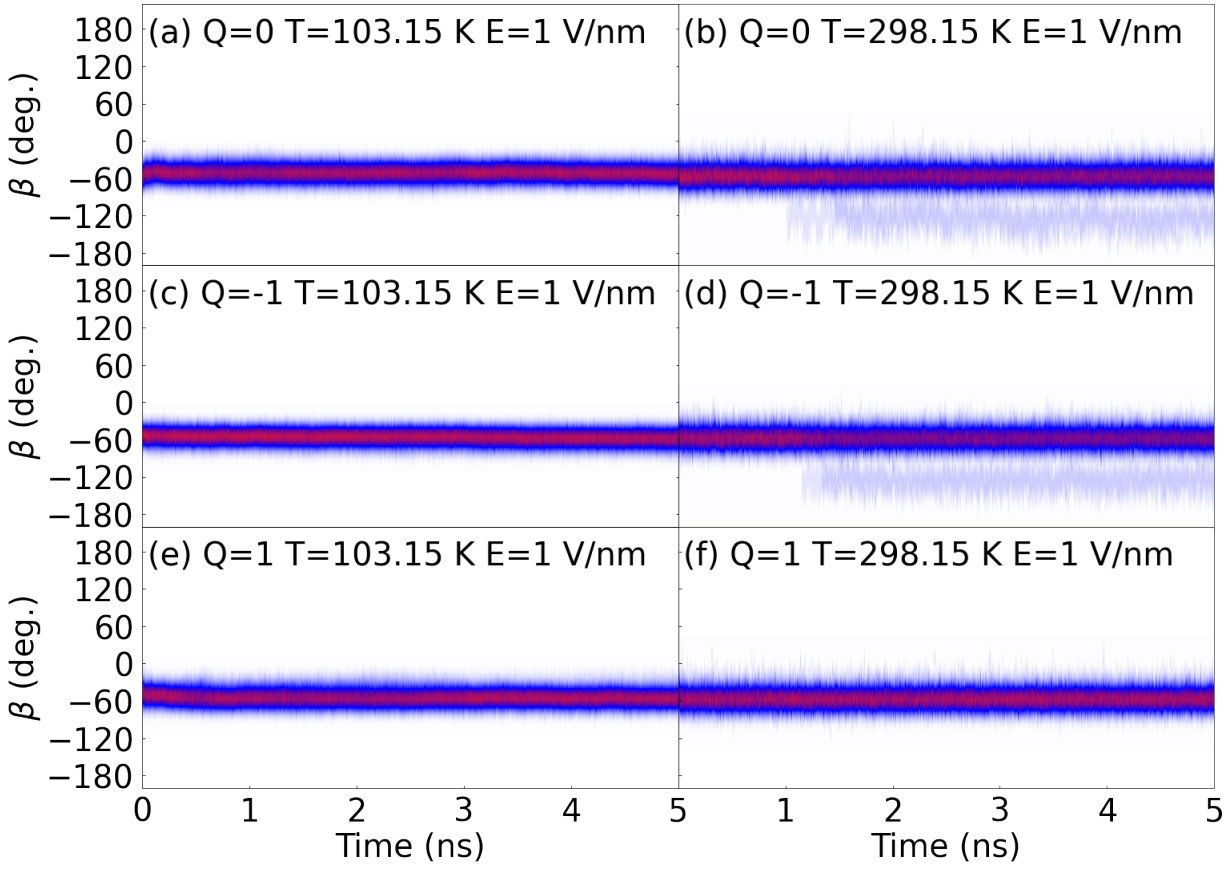

Figure S6: Time-resolved evolution of torsion β under different conditions in **M1** (a) Q=0 T=103.15 K E=1 V/nm, (b) Q=0 T=298.15 K E=1 V/nm, (c) Q=-1 T=103.15 K E=1 V/nm, (d) Q=-1 T=298.15 K E=1 V/nm, (e) Q=1 T=103.15 K E=1 V/nm, (f) Q=1 T=298.15 K E=1 V/nm.

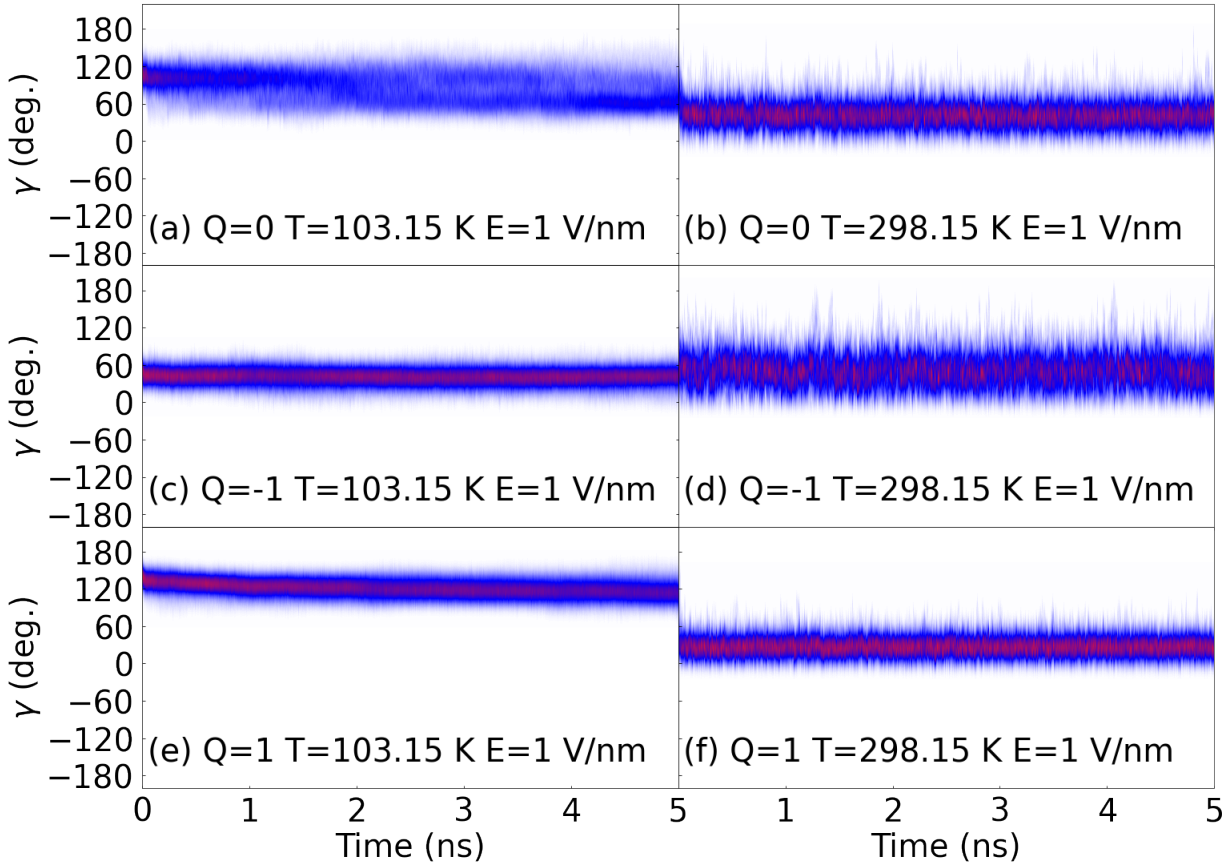

Figure S7: Time-resolved evolution of torsion γ under different conditions in **M1** (a) Q=0 T=103.15 K E=1 V/nm, (b) Q=0 T=298.15 K E=1 V/nm, (c) Q=-1 T=103.15 K E=1 V/nm, (d) Q=-1 T=298.15 K E=1 V/nm, (e) Q=1 T=103.15 K E=1 V/nm, (f) Q=1 T=298.15 K E=1 V/nm.

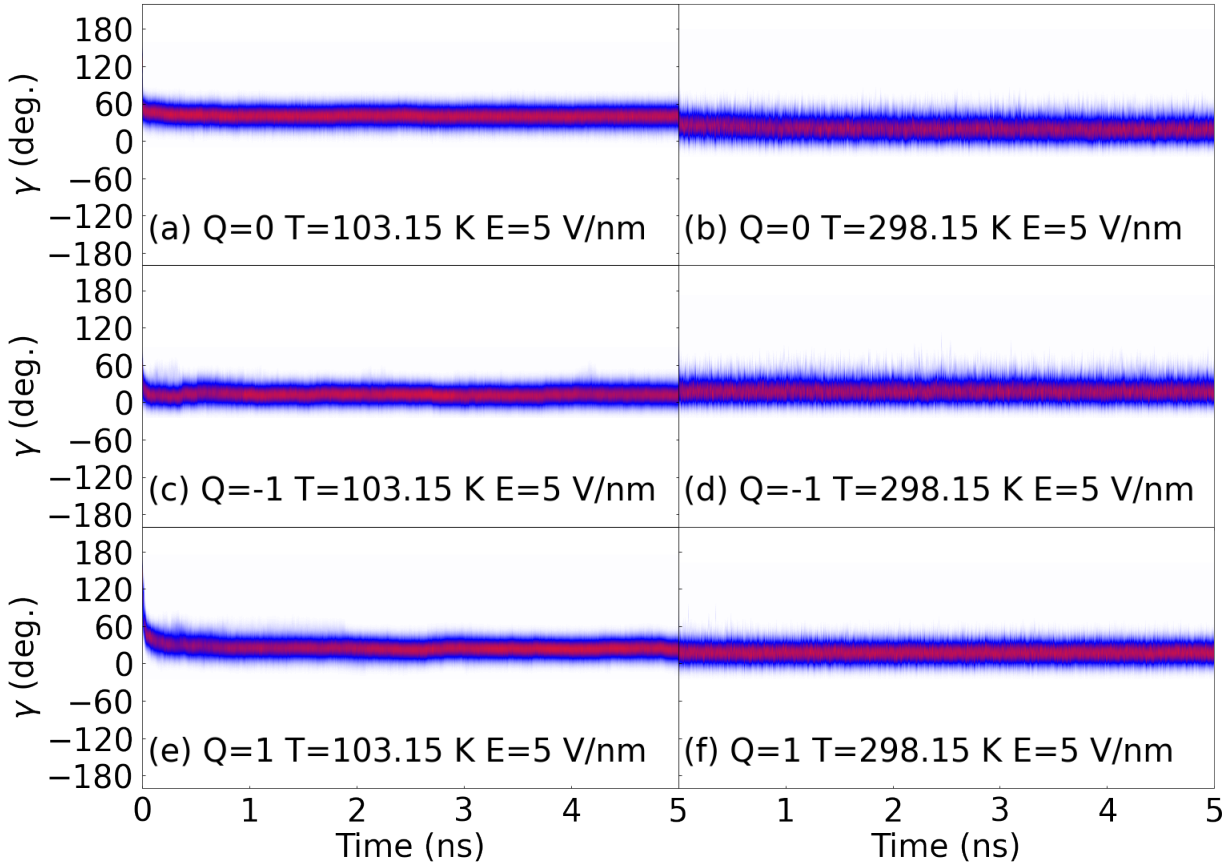

Figure S8: Time-resolved evolution of γ under different conditions in **M1** (a) Q=0 T=103.15 K E=5 V/nm, (b) Q=0 T=298.15 K E=5 V/nm, (c) Q=-1 T=103.15 K E=5 V/nm, (d) Q=-1 T=298.15 K E=5 V/nm, (e) Q=1 T=103.15 K E=5 V/nm, (f) Q=1 T=298.15 K E=5 V/nm.

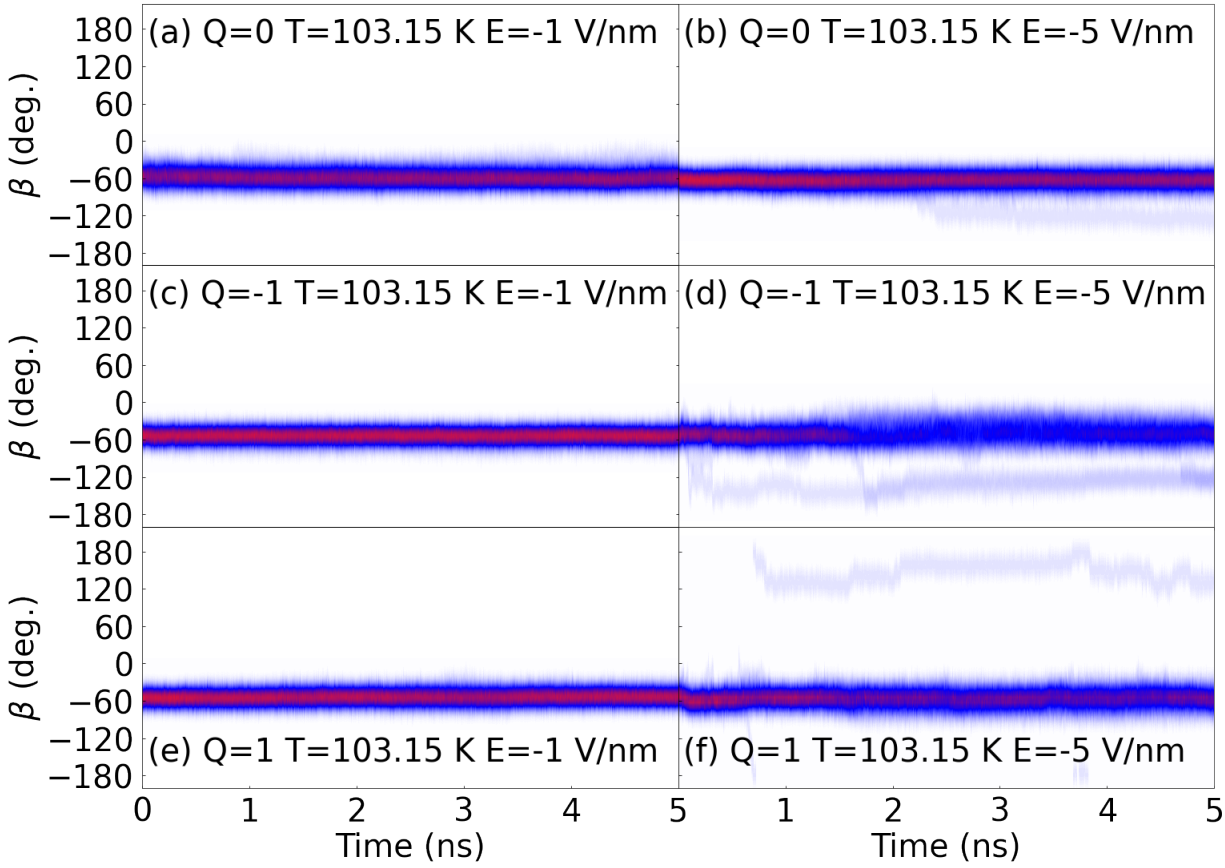

Figure S9: Time-resolved evolution of torsion β under different conditions in **M1** (a) Q=0 T=103.15 K E=-1 V/nm, (b) Q=0 T=103.15 K E=-5 V/nm, (c) Q=-1 T=103.15 K E=-1 V/nm, (d) Q=-1 T=103.15 K E=-5 V/nm, (e) Q=1 T=103.15 K E=-1 V/nm, (f) Q=1 T=103.15 K E=-5 V/nm.

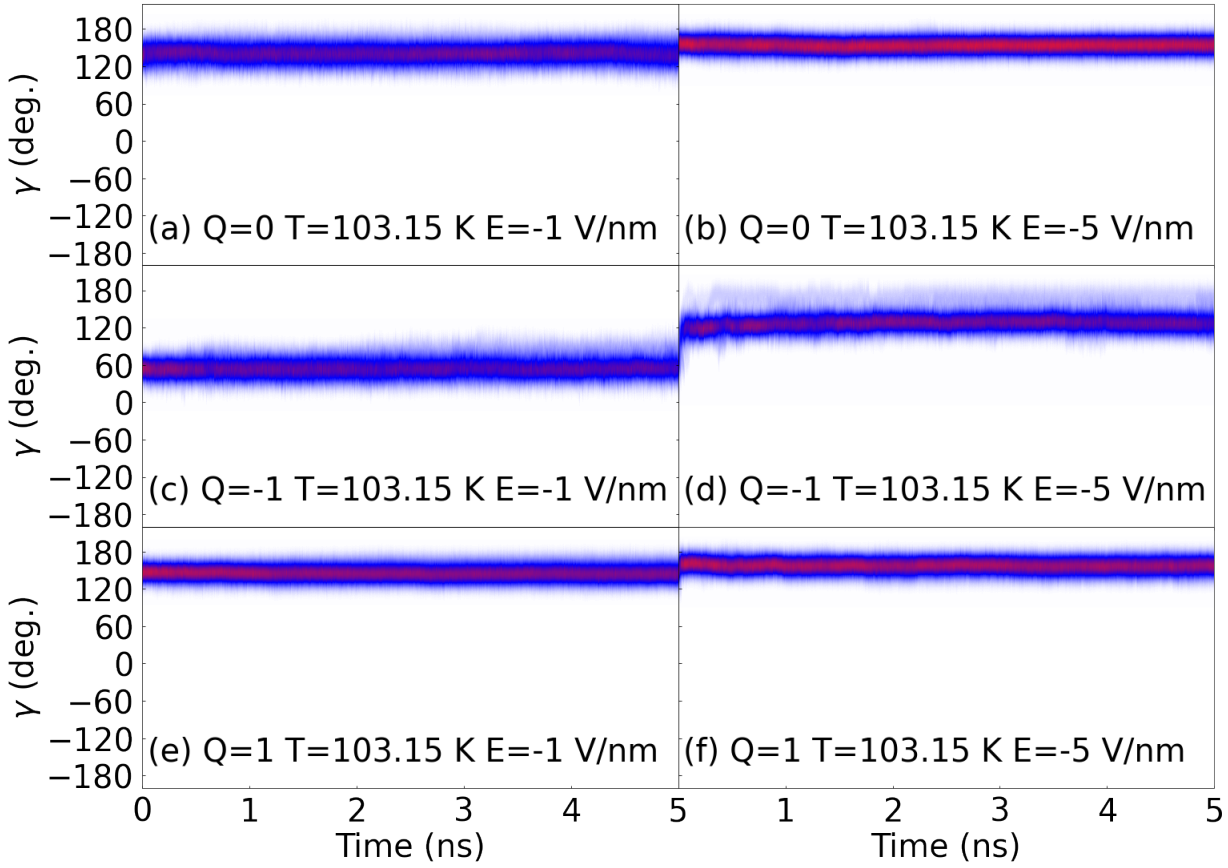

Figure S10: Time-resolved evolution of torsion γ under different conditions in **M1** (a) Q=0 T=103.15 K E=-1 V/nm, (b) Q=0 T=103.15 K E=-5 V/nm, (c) Q=-1 T=103.15 K E=-1 V/nm, (d) Q=-1 T=103.15 K E=-5 V/nm, (e) Q=1 T=103.15 K E=-1 V/nm, (f) Q=1 T=103.15 K E=-5 V/nm.

The simulation results of M2 under different conditions

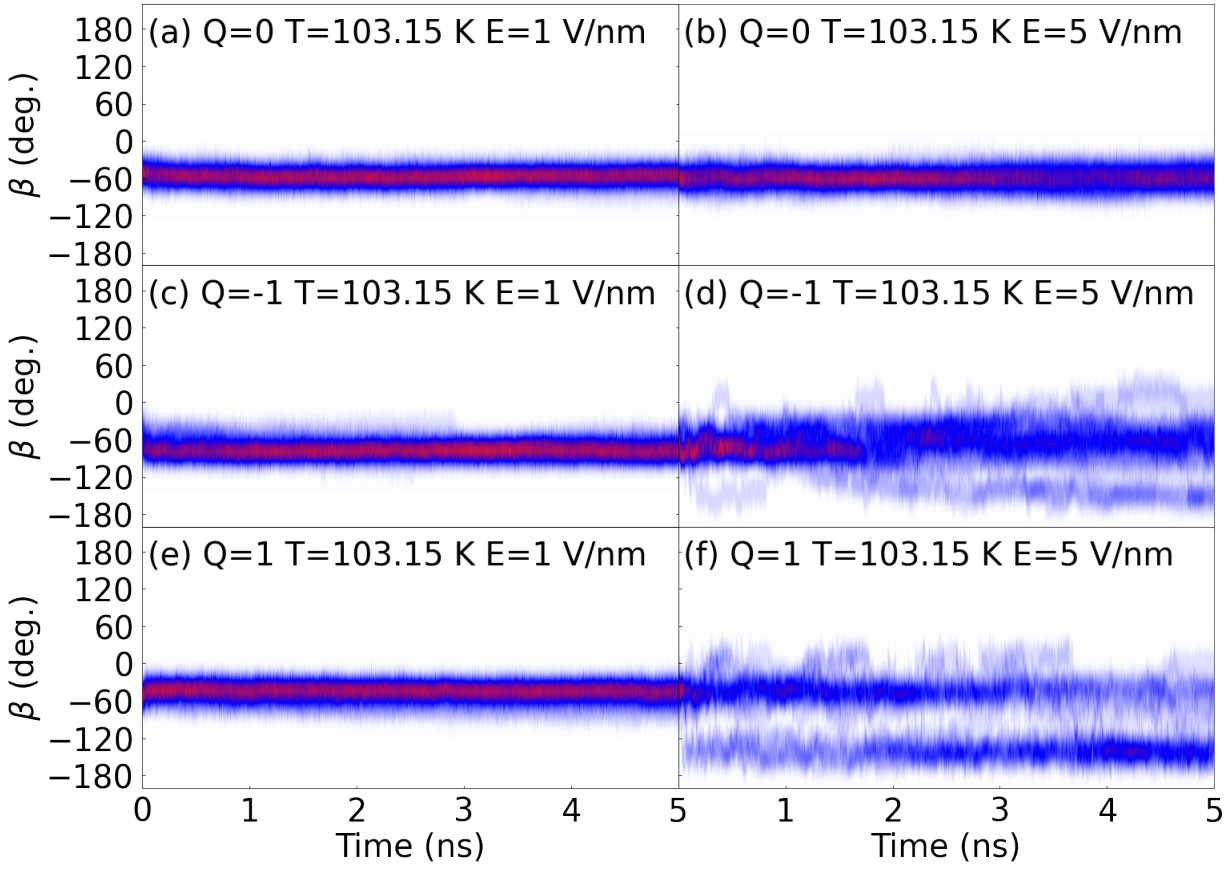

Figure S11: Time-resolved evolution of torsion β under different conditions in **M2** (a) Q=0 T=103.15 K E=1 V/nm, (b) Q=0 T=103.15 K E=5 V/nm, (c) Q=-1 T=103.15 K E=1 V/nm, (d) Q=-1 T=103.15 K E=5 V/nm, (e) Q=1 T=103.15 K E=1 V/nm, (f) Q=1 T=103.15 K E=5 V/nm.

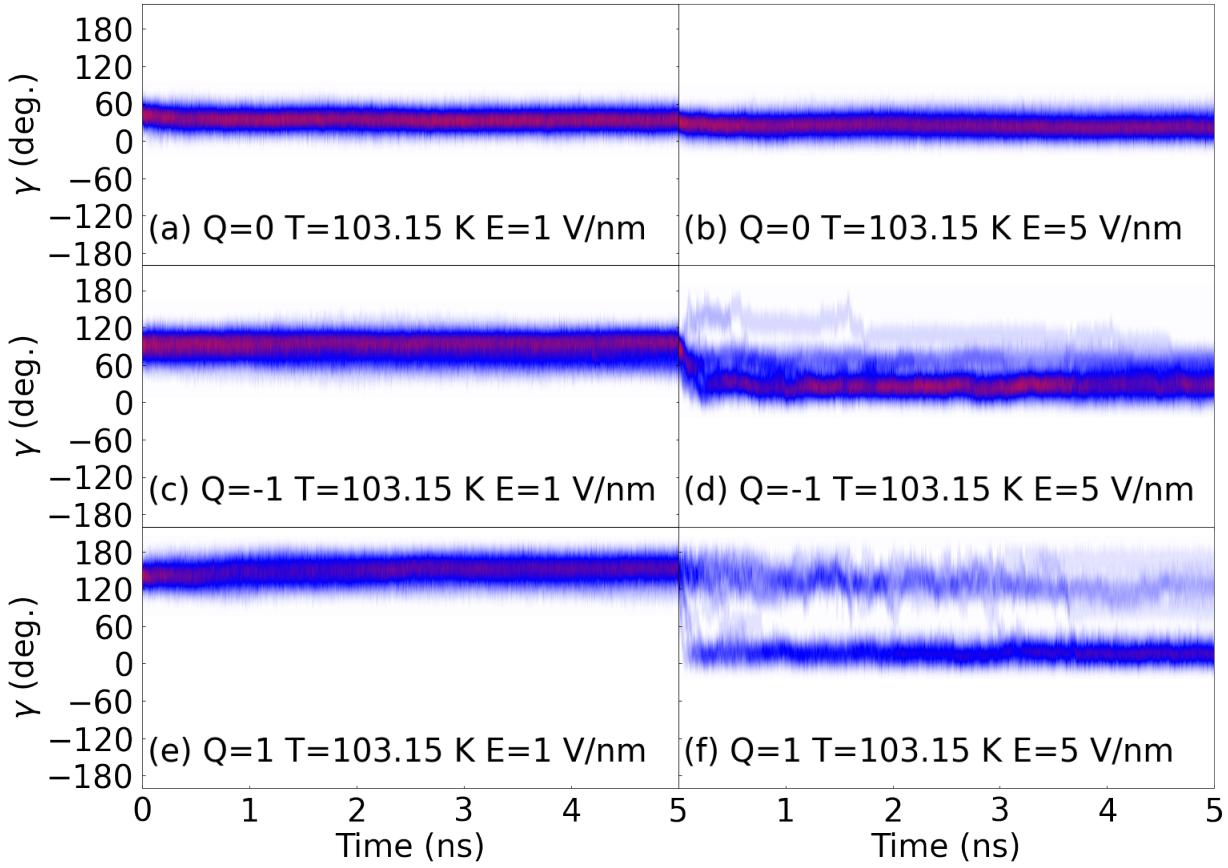

Figure S12: Time-resolved evolution of torsion γ under different conditions in **M2** (a) Q=0 T=103.15 K E=1 V/nm, (b) Q=0 T=103.15 K E=5 V/nm, (c) Q=-1 T=103.15 K E=1 V/nm, (d) Q=-1 T=103.15 K E=5 V/nm, (e) Q=1 T=103.15 K E=1 V/nm, (f) Q=1 T=103.15 K E=5 V/nm.

The simulation results of M3 under different conditions

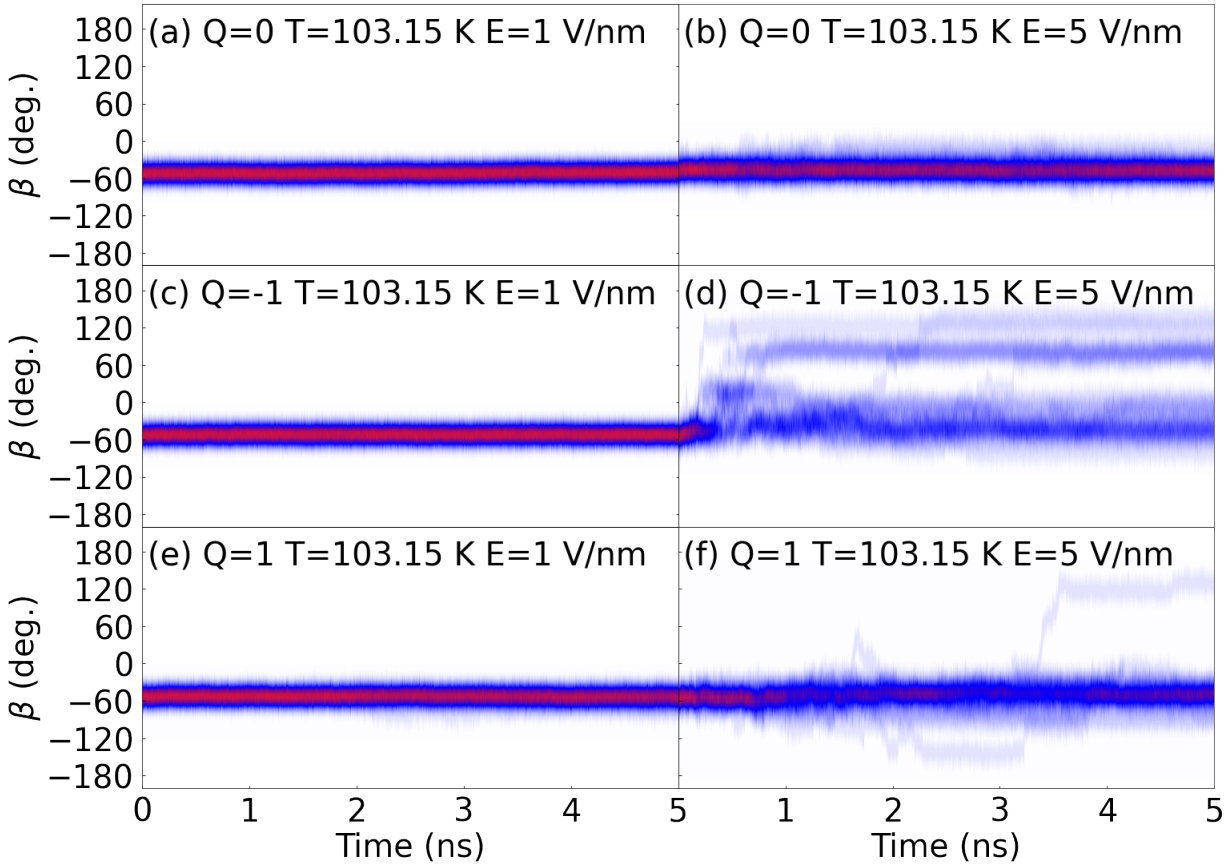

Figure S13: Time-resolved evolution of torsion β under different conditions in **M3** (a) Q=0 T=103.15 K E=1 V/nm, (b) Q=0 T=103.15 K E=5 V/nm, (c) Q=-1 T=103.15 K E=1 V/nm, (d) Q=-1 T=103.15 K E=5 V/nm, (e) Q=1 T=103.15 K E=1 V/nm, (f) Q=1 T=103.15 K E=5 V/nm.

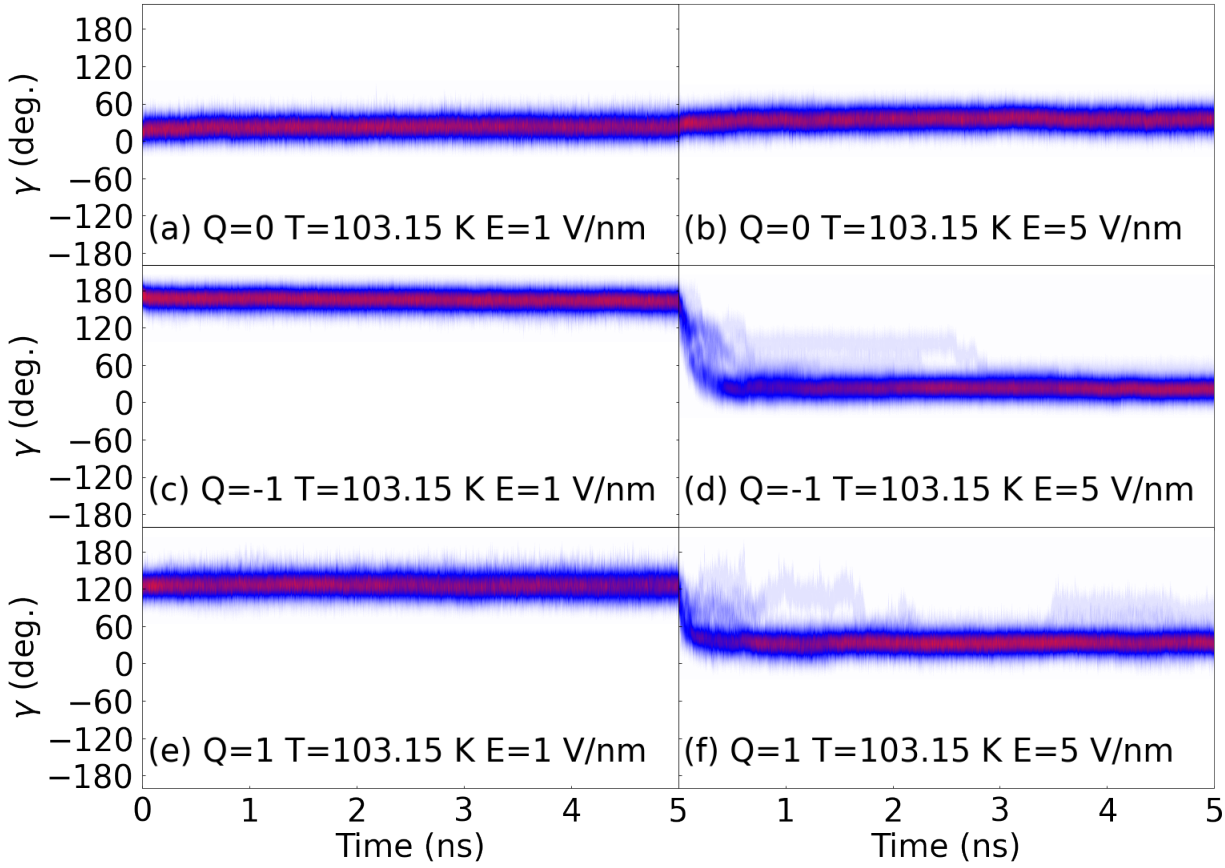

Figure S14: Time-resolved evolution of torsion γ under different conditions in **M3** (a) Q=0 T=103.15 K E=1 V/nm, (b) Q=0 T=103.15 K E=5 V/nm, (c) Q=-1 T=103.15 K E=1 V/nm, (d) Q=-1 T=103.15 K E=5 V/nm, (e) Q=1 T=103.15 K E=1 V/nm, (f) Q=1 T=103.15 K E=5 V/nm.

The simulation results of M4 under different conditions

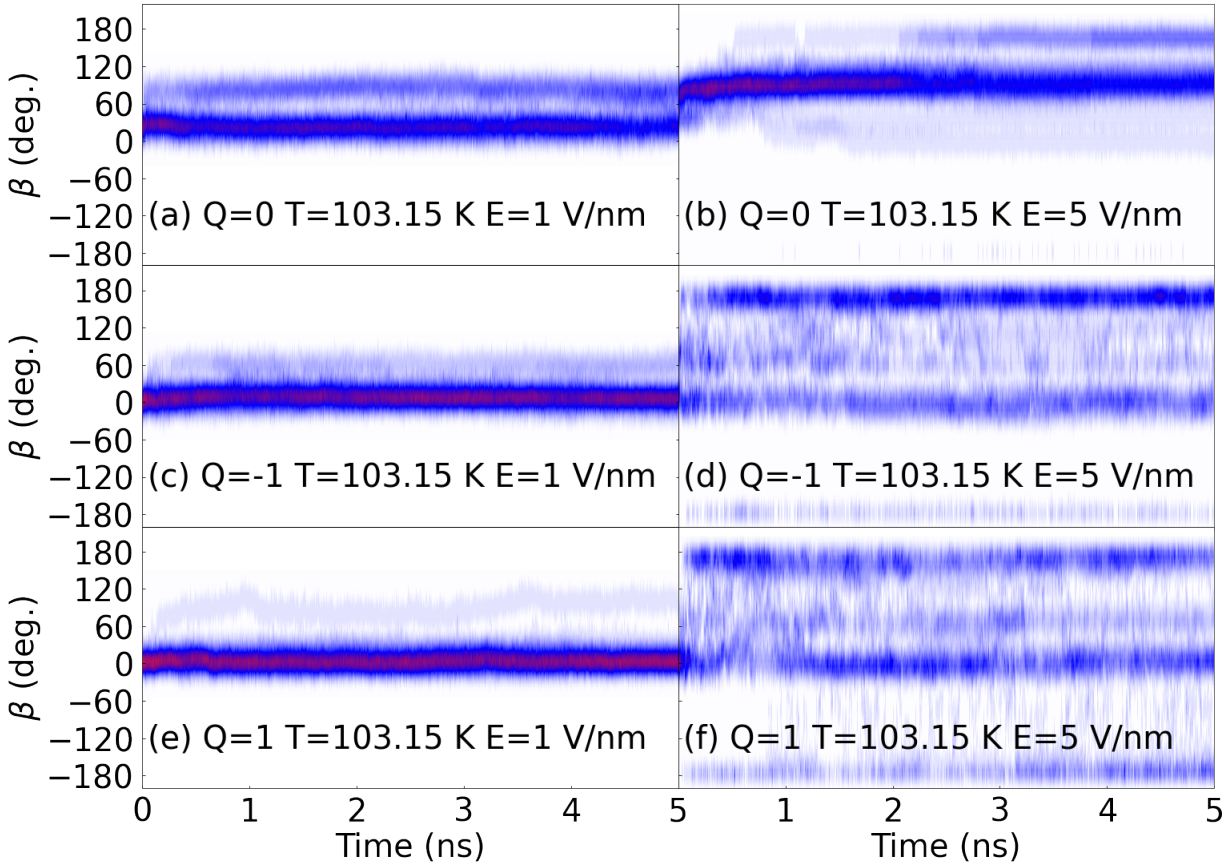

Figure S15: Time-resolved evolution of torsion β under different conditions in **M4** (a) Q=0 T=103.15 K E=1 V/nm, (b) Q=0 T=103.15 K E=5 V/nm, (c) Q=-1 T=103.15 K E=1 V/nm, (d) Q=-1 T=103.15 K E=5 V/nm, (e) Q=1 T=103.15 K E=1 V/nm, (f) Q=1 T=103.15 K E=5 V/nm.

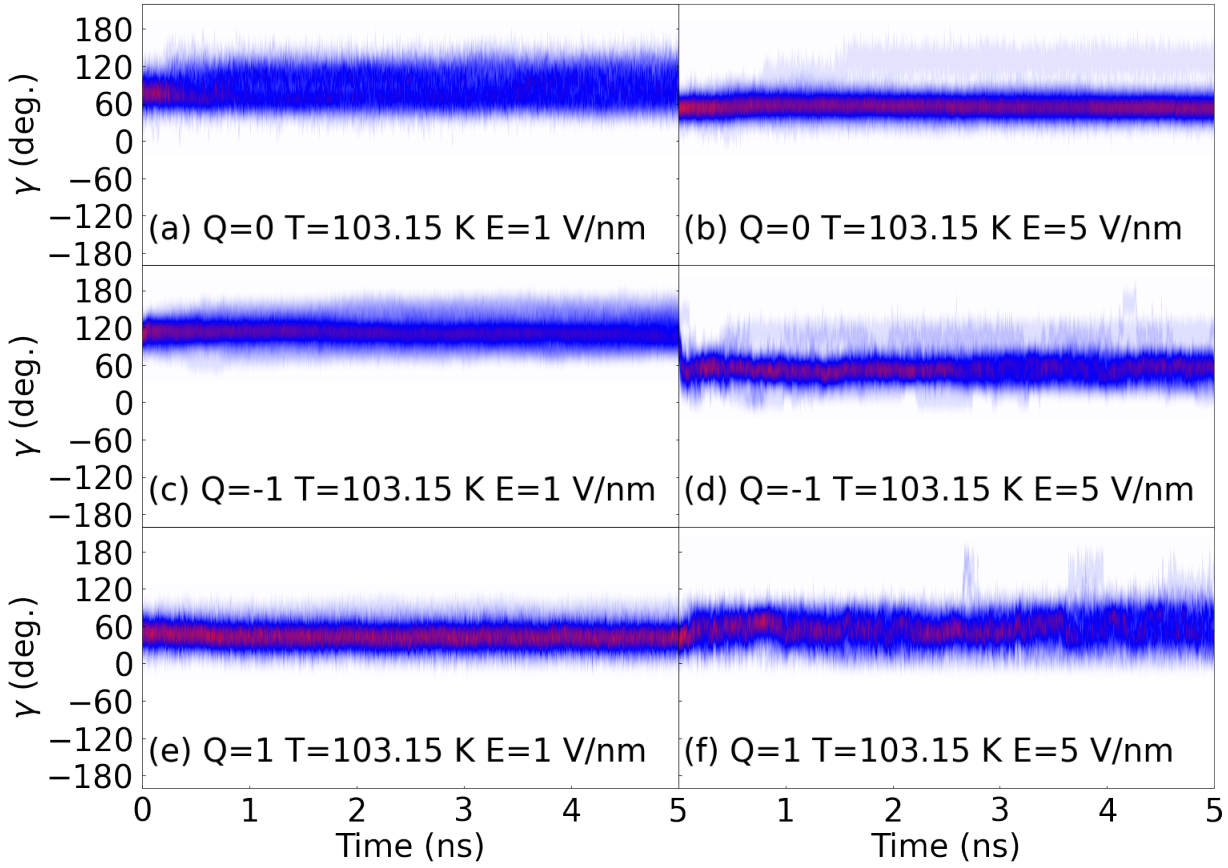

Figure S16: Time-resolved evolution of torsion γ under different conditions in **M4** (a) Q=0 T=103.15 K E=1 V/nm, (b) Q=0 T=103.15 K E=5 V/nm, (c) Q=-1 T=103.15 K E=1 V/nm, (d) Q=-1 T=103.15 K E=5 V/nm, (e) Q=1 T=103.15 K E=1 V/nm, (f) Q=1 T=103.15 K E=5 V/nm.

References

(1) Xu, H.; Zhang, B.; Tao, Y.; Xu, W.; Hu, B.; Yan, F.; Wen, J. *J. Phys. Chem. A* **2023**, *127*, 7682–7693.

(2) Neese, F. *Wiley Interdiscip. Rev.: Comput. Mol. Sci.* **2022**, *12*, e1606.

(3) Wang, J.; Wolf, R. M.; Caldwell, J. W.; Kollman, P. A.; Case, D. A. *J. Comput. Chem.* **2004**, *25*, 1157–1174.

(4) Bayly, C. I.; Cieplak, P.; Cornell, W.; Kollman, P. A. *J. Phys. Chem* **1993**, *97*, 10269–10280.

(5) Becke, A. D. *J. Chem. Phys* **1993**, *98*, 1372–1377.

(6) A smooth particle mesh Ewald method. *J. Chem. Phys* **1995**, *103*, 8577–8593.

(7) Hess, B.; Bekker, H.; Berendsen, H. J.; Fraaije, J. G. *J. Comput. Chem.* **1997**, *18*, 1463–1472.

(8) Bussi, G.; Donadio, D.; Parrinello, M. *The Journal of chemical physics* **2007**, *126*.

(9) Berendsen, H. J.; Postma, J. v.; Van Gunsteren, W. F.; DiNola, A.; Haak, J. R. *J. Chem. Phys* **1984**, *81*, 3684–3690.

(10) Berendsen, H. J.; van der Spoel, D.; van Drunen, R. *Comput. Phys. Commun.* **1995**, *91*, 43–56.

(11) Humphrey, W.; Dalke, A.; Schulten, K. *J. Mol. Graphics* **1996**, *14*, 33–38.